

Local electronic transport in $\text{La}_{0.7}\text{Sr}_{0.3}\text{MnO}_3$ thin films studied by scanning tunneling potentiometry

B. Grévin,¹ I. Maggio-Aprile,¹ A. Bentzen,¹ L. Ranno,² A. Llobet,² and Ø. Fischer¹

¹DPMC, Université de Genève, 24 quai Ernest Ansermet, CH1211-Genève, Switzerland

²Laboratoire Louis Néel, CNRS, 25 avenue des Martyrs, BP 166, 38042 Grenoble Cedex 09, France

(Received 11 February 2000)

We have used a scanning tunneling microscope in potentiometry mode to investigate the local electric potential distribution in current carrying epitaxial $\text{La}_{0.7}\text{Sr}_{0.3}\text{MnO}_3$ thin films, with magnetotransport properties similar to the ones of single crystals. Scans imaging simultaneously the surface topography and the potential distribution have been obtained with an unprecedented resolution. In textured $\text{La}_{0.7}\text{Sr}_{0.3}\text{MnO}_3/\text{MgO}$, sharp potential steps coincide with some of the grain boundaries, whereas other grains are electrically well connected. The precise nature of the local electronic transport, the percolation of the current through the grain network, and the existence of phase separated insulating domains are then discussed.

There is increasing interest in the study of natural¹⁻⁵ or artificial⁶⁻⁸ grain boundaries in manganese perovskites $R_{1-x}A_x\text{MnO}_3$, as their low-field magnetoresistance response (LFMR) amplitude is known to be intimately related to the presence of interfaces. In the case of $\text{La}_{1-x}\text{Sr}_x\text{MnO}_3$ thin films, LFMR effects have been found in films deposited on polycrystalline³ or bicrystal^{7,8} SrTiO_3 substrates, and also in polycrystalline $\text{La}_{0.7}\text{Sr}_{0.3}\text{MnO}_3/\text{MgO}$ films grown on mismatched single crystalline MgO substrates.⁵ Epitaxial and polycrystalline $\text{La}_{0.7}\text{Sr}_{0.3}\text{MnO}_3/\text{MgO}$ films were obtained by Ranno *et al.* depending on the substrate temperature.⁵ The epitaxial films (with grains textured along [100] directions for $\text{La}_{0.7}\text{Sr}_{0.3}\text{MnO}_3/\text{MgO}$) exhibit magnetotransport properties similar to that recorded in single crystals (the expression ‘‘single-crystal like’’ refer here to such properties). The absolute value of the resistivity may be somewhat higher than in single crystals, but has the same temperature- and magnetic-field dependence: these films are metallic in the low-temperature ferromagnetic phase, and the so-called colossal magnetoresistance is significant only near the Curie temperature. In contrast, the transport properties of the polycrystalline films (for which the grains grow without any crystallographic relation with the substrate) are quite different. The absolute value of their resistivity is several orders of magnitude higher, and the T dependence of the resistivity is determined by intergrain conduction. The resistivity then displays a nonmonotonic behavior in the ferromagnetic phase, and presents a low- T increase associated with localization effects. Moreover, a strong LFMR effect (or intergrain magnetoresistance, IMR) is observed at low temperatures.

In the case of $\text{La}_{1-x}\text{Sr}_x\text{MnO}_3/\text{MgO}$ thin films, a striking question concerns the absence of an intermediate transport regime between the single-crystal like magnetotransport shown by textured samples, and the low-field IMR regime of polycrystalline mismatched films. This well-marked frontier between both regimes is rather surprising, as it is possible to vary continuously the deposition conditions from textured to polycrystalline samples.⁵ We underline here that the precise nature of the local electronic transport through the grain network of textured samples is a nontrivial question. Indeed, to

account for their single-crystal-like transport properties, one shall assume a negligible contribution of grain boundaries to the resistivity. Nevertheless, it is widely accepted that the grain boundaries increase significantly the macroscopic resistivity of thin films. This raises the question of the differences between intergrain transport in textured and polycrystalline samples. So far, as macroscopic transport measurements cannot really answer correctly these questions, a correct picture of the electronic transport in these films is still missing.

To really understand these features, it is necessary to study the transport properties using local probes. This can be done by using scanning tunneling potentiometry⁹ (STP), which gives a direct measurement of the local electric potential distribution under current flow.

In this study, we have performed STP measurements with an unprecedented spatial resolution, on epitaxial $\text{La}_{0.7}\text{Sr}_{0.3}\text{MnO}_3/\text{MgO}$ thin films with single-crystal-like macroscopic transport properties, despite a *non-negligible density of grain boundaries between crystallites*. The scanning tunneling microscope (STM) was used to image both the topography and the local electric potential in a current-carrying line patterned on the sample. Both topographic and potentiometric images obtained present extremely well resolved features, which allow a careful analysis of the electronic transport. Sharp steps in the electric potential are unambiguously related to the presence of grain boundaries, whereas some grains are ‘‘electrically well connected’’ without any potential drop at their boundaries. In the light of these results, we discuss the existence of a percolation mechanism for the current through the grain network, and the differences in the intergrain transport between epitaxial and polycrystalline samples.

For this work, a 60-nm-thick epitaxial $\text{La}_{0.7}\text{Sr}_{0.3}\text{MnO}_3$ thin film on MgO (001) (textured along the three axes) was grown by pulsed laser deposition, with the deposition parameters used in Ref. 5 for high-temperature-grown epitaxial samples. The transport properties of such a sample are extensively described in Ref. 5. We thus only underline that the T dependence of its resistivity (four points measurements,

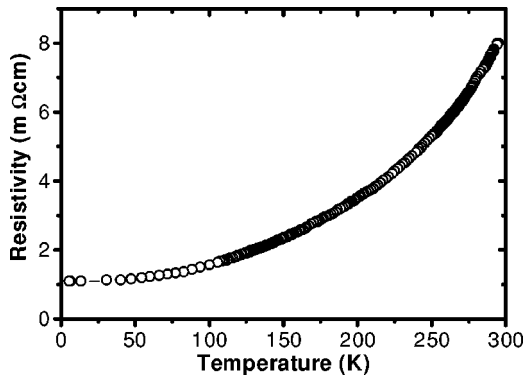


FIG. 1. Temperature dependence of the resistivity of the $\text{La}_{0.7}\text{Sr}_{0.3}\text{MnO}_3/\text{MgO}$ epitaxial thin film investigated in this study.

see Fig. 1) is single-crystal like, and that the low- T resistivity is two orders of magnitude lower than in the case of polycrystalline samples ($\rho_0 \sim 300$ m Ω cm at 4.2 K in Ref. 5).

The STP measurements were performed at room temperature on a 20- μm narrow and 0.5-mm long line (see Fig. 2A), patterned on the film using a standard lithographic process. The sample was cleaned in acetone (in an ultrasonic bath) and annealed under 500 mbars of pure oxygen for 10 h in a deposition chamber, with the aim to restore the surface quality after the lithographic process. The total resistance of this

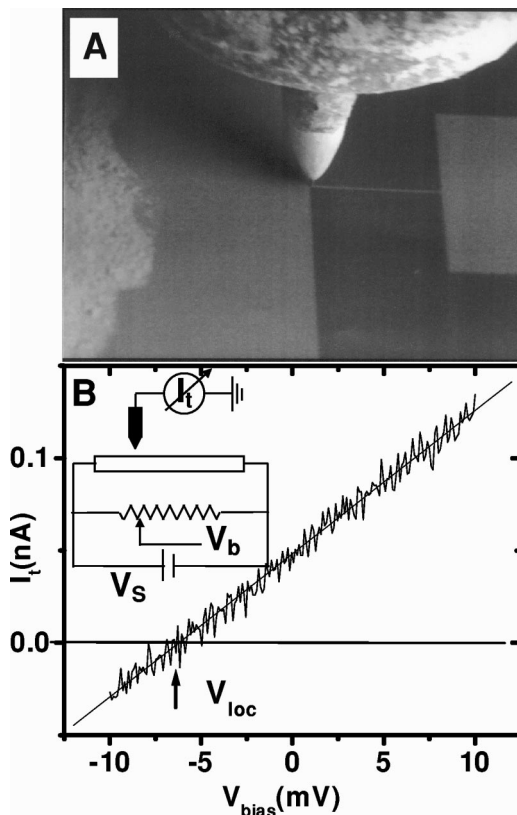


FIG. 2. (A) Scanning electron microscope image showing the coarse approach of the STM tip on the 20- μm narrow patterned line. The dc voltage V_S is applied between the ground electrode (at left) and the potential electrode (at right). (B) Typical $I_t(V_b)$ curve showing the interpolation of the local potential V_{loc} value (corresponding to $I_t=0$). The inset shows the circuit used for scanning tunneling potentiometry in this study.

line after annealing is 35 k Ω (at 300 K), corresponding to a resistivity value of 8 m Ω cm. The sample was then transferred in an UHV-analysis chamber (base pressure $< 10^{-10}$ mbars) equipped with a scanning electron microscope and a STM. Last, the T dependence of the resistivity was measured *ex situ* after the STP measurements.

The STP technique used here is described in detail in Ref. 10, and we will here restrict our presentation to some specific points. A dc voltage V_S is applied between the two extremities of the sample, designated here as the ground electrode and the potential electrode (Fig. 2A). To measure simultaneously the topography and the local electric potential V_{loc} , a bias voltage V_b is introduced relative to the tip (grounded) at an electrically equivalent point under the tip by a bridge circuit (see the insert of Fig. 2B). Topography is acquired in a constant current mode at relatively high bias ($V_b = +0.6$ V in this study). Then, the feedback loop is suspended and measurements of the tunneling current I_t are made by sweeping V_b from values below to above V_{loc} . Linear interpolation of the bias value V_b for which $I_t=0$ then gives a direct measure of V_{loc} . This potential measurement was done after reducing the bias voltage ($V_b = +50$ mV) before opening the feedback loop, in order to decrease the tunnel resistance and increase the signal to noise ratio of the $I_t(V_b)$ curves. Fifty spectra were averaged to interpolate each pixel of potentiometry data. A typical $I_t(V_b)$ characteristic obtained during a potentiometric scan is displayed in Fig. 2B. For low bias values, the $I_t(V_b)$ curves display a perfect linearity, which enables accurate interpolations of V_{loc} .

Let us now consider a potentiometric two-dimensional (2D) image on a 2000×2000 - \AA region with an average field +17.6 V/mm (applied from right to left) on the sample, displayed in Fig. 3B, with the corresponding topographic image in Fig. 3A. Both images consist of 50×50 pixels of information, and the absolute scale for potentiometric data is 4 mV from black (low potential) to white (high potential). The local potential increases from left to right in good agreement with the average field direction. On the topographic image, very distinct grains appear, separated by boundaries revealed by more or less sharp topographic features. To our knowledge, both electric potential and topography were never simultaneously so precisely imaged in the case of manganites or high- T_C superconducting thin films.

One of the most remarkable features is the frequent presence of sharp potential steps associated with the grain boundaries. Besides these features, the potentiometric image shows large plateaus where the potential varies smoothly. Some grains seem then to be “electrically well connected” with good metallic contact, as some intergrain regions display no potential steps in the corresponding part of the potentiometric image.

This case is illustrated by the cross sections displayed in Fig. 4. On the upper cross section (Fig. 4A) with a total drop $\Delta V_{loc} = 1.5$ mV across the 2000- \AA -long potentiometric trace, only one pair of grains is badly connected, whereas the three following grains (viewing the image from the left to the right part) are well connected. This ΔV_{loc} value is much lower than the average drop that one should observe over 2000 \AA if the potential drop was uniform in this film:

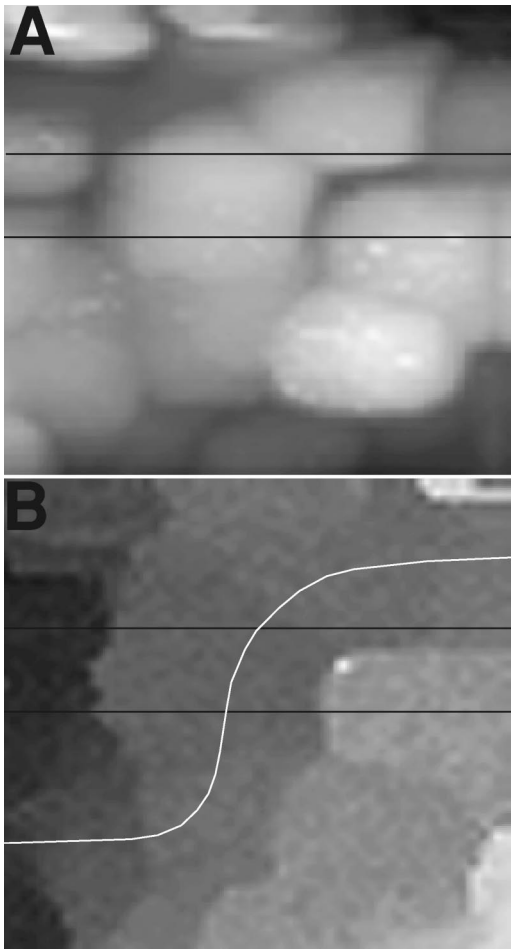


FIG. 3. (A) Topographic and (B) potentiometric gray scale 2000×2000 -Å images of $\text{La}_{0.7}\text{Sr}_{0.3}\text{MnO}_3/\text{MgO}$ epitaxial thin film acquired simultaneously with an applied electric field of 17.6 V/mm. The gray scale for topography covers a range of 177 Å from black (low) to white (high) with a rms value of 30 Å. The absolute scale for potentiometric data is 4 mV from black (low potential) to white (high potential). The black lines indicate the positions of the cross sections displayed in Figs. 4A and B, the white line presents a possible percolation path for the current (see the text).

$\Delta V_{mean} = 3.5$ mV. We also note that the slope inside the grain is about 1/5 of the average potential gradient. The middle cross section (Fig. 4B) shows two pairs of badly connected grains, with a larger total drop $\Delta V_{loc} = 2$ mV. A third 2000 -Å cross section (Fig. 4C), was extracted from a 2D potentiometric image (not displayed) taken at another part of the sample, before and after reversing the sign of the applied voltage V_S . Here, we observe several potential steps corresponding to three neighboring pairs of badly connected grains, and the total potential drop $\Delta V_{loc} = 3.4$ mV is there almost equal to the average value $\Delta V_{mean} = 3.5$ mV. At this stage, it seems very likely that *an important part of the potential drops occurs at the grain boundaries* in this film, as several badly connected grains are needed to reach the average value for ΔV_{loc} . Besides this result, we observe in this last cross section a reversal in V_{loc} variations, corresponding to the inversion of V_S polarity, which definitely confirms that the measured local potential is directly related to the applied voltage on the sample.

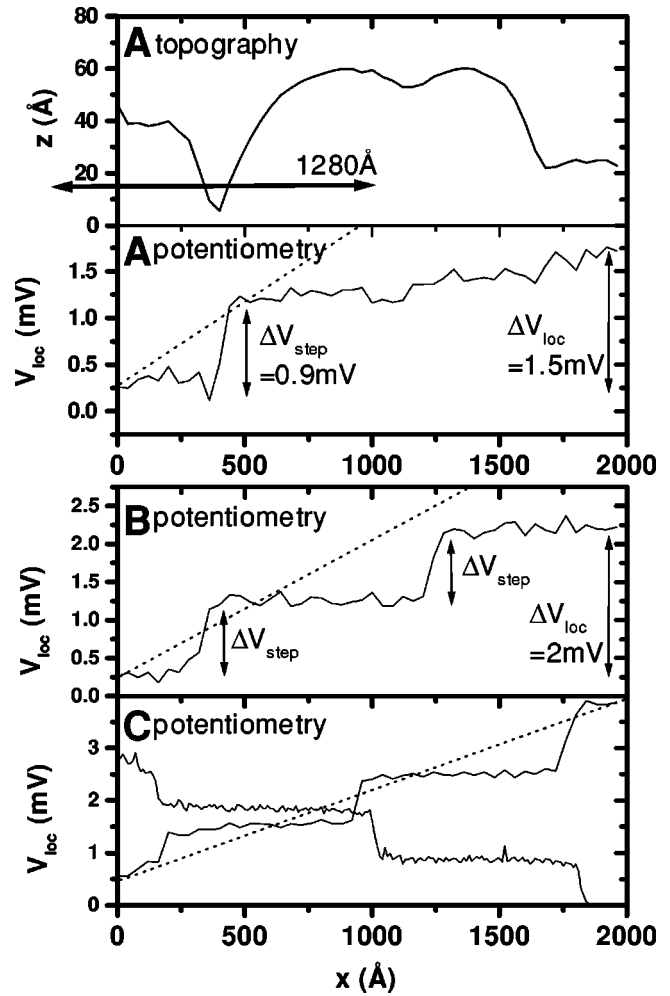


FIG. 4. (A) and (B) Single line cross sections extracted from Fig. 3. (A) both topographic (upper part) and potentiometric data (lower part) are displayed. The arrow indicates what would be the distance of a hypothetical tip jump (see the text). (C) Single line potentiometric cross section taken in another part of the sample, before and after reversing the direction of the applied voltage V_S . The uniform potential distribution ΔV_{mean} (dotted lines) expected for the applied field is shown in A, B, and C.

Before going further in the analysis of the local electronic transport, it is now necessary to discuss whether the potential drops are due to intrinsic intergrain resistivity, or if they are artifacts due to a discontinuous change in the tunneling position during the scan over the grain boundary.¹⁰ For example, let us consider the first cross section with only one step in the potential, with an amplitude $\Delta V_{step} = 0.9$ mV. For this cross section, both topographic (top part of Fig. 4A) and potentiometric plots (bottom part of Fig. 4A) are displayed, and an arrow indicates what would be the distance of such a discontinuous change in the tunneling position (also called “tip jump”), assuming that the real potential drop in the film is uniform. The total drop over the 2000 -Å length is $\Delta V_{loc} = 1.5$ mV, the ΔV_{step} value should then correspond to a tip jump on a distance of $(0.9/1.5) \times 2000 = 1285$ Å. Such a tip jump would actually imply that the sample is “imaging” the tip,¹⁰ which is highly incompatible with the excellent resolution of the topographic image, which does not display the typical aspect of identical features re-

produced systematically during the scan in the case of “tip imaging.” Moreover, we have already noticed that a certain number of potential drops are needed to reach the expected mean value for ΔV_{loc} on the potentiometric cross sections. As previously mentioned, *this strongly supports the idea that the major part of the real potential drop occurs across the grain boundaries*, so that the sharp steps are intrinsically linked to the local electronic transport properties of the thin film. For all these reasons, we are confident that the potentiometric images discussed here reflect the real local potential distribution in the thin film.

Now we want to discuss the implications of these results concerning the microscopic factors determining the nature of the electronic transport in $\text{La}_{0.7}\text{Sr}_{0.3}\text{MnO}_3$ thin films. The previous analysis of V_{loc} topology suggests an important contribution of grain boundaries to the global resistivity (at 300 K), although the macroscopic transport remains single-crystal like in our $\text{La}_{0.7}\text{Sr}_{0.3}\text{MnO}_3/\text{MgO}$ thin film. An explanation which comes naturally, is that the transport proceeds via a percolation of the current through the “electrically well connected” crystallites evidenced by the STP imaging. Considering the STP image, it is actually possible to follow some topologic paths from right to left, without meeting well marked drops in V_{loc} (a possible path is proposed in Fig. 3B). In such a percolating picture, the T dependence of the resistivity is in majority due to the intrinsic contributions of crystallites, and is therefore similar to the one found in single crystals. Moreover, as the current is strongly blocked between certain badly connected grains, the global resistivity is not directly related to the high resistance of the boundaries separating the latter grains, but rather to the restricted geometry of the percolation path. In this context, we can estimate from our results an average *effective* grain boundary resistance in the range $0.3 \times 10^{-7} \Omega \text{ cm}^2$ to $0.8 \times 10^{-7} \Omega \text{ cm}^2$. It is here of interest to note that in a previous STP study, Versluijs *et al.* reported GB resistivities one or two order of magnitude higher for polycrystalline $\text{La}_{0.7}\text{Sr}_{0.3}\text{MnO}_3$ films.¹¹

In their study,¹¹ the authors claimed that sharp potential steps were only present in the case of polycrystalline $\text{La}_{0.7}\text{Sr}_{0.3}\text{MnO}_3/\text{MgO}$ thin films, whereas such steps were totally absent in the case of epitaxial $\text{La}_{0.7}\text{Sr}_{0.3}\text{MnO}_3/\text{MgO}$

samples with an intrinsic homogeneous single-crystal-like transport. Our results force us to reconsider this picture. The authors analyzed the local potential in a very low-resistive epitaxial thin film, with a residual resistivity one order of magnitude lower than that of our sample ($\rho_0 = 100 \mu\Omega \text{ cm}$ in their work¹¹ and $\rho_0 = 1 \text{ m}\Omega \text{ cm}$ in our study). Indeed, in such a very low-resistive sample, the major part of the crystallites should be electrically well connected, thus leading to a more homogeneous electronic transport.

Next, it is important to realize that our analysis points to the existence of a percolation threshold for the current in $\text{La}_{0.7}\text{Sr}_{0.3}\text{MnO}_3/\text{MgO}$ thin films. When varying the synthesis conditions from epitaxial to polycrystalline samples, the average misorientation angle between grains increases, and the crystallites become less connected. Below a certain percolation threshold, the macroscopic transport properties get therefore suddenly dominated by intergrain transport, whereas the transport remains single-crystal like above the percolation threshold. This consistently accounts for the absence of an intermediate regime between single-crystal-like and polycrystalline-like electronic transport.

Last, it is also interesting to consider our results in the frame of recent STS results¹² reported for $\text{La}_{0.7}\text{Ca}_{0.3}\text{MnO}_3$, and presented in favor of phase separation between metallic and more insulating clusters on a submicronic scale. In the case of textured $\text{La}_{0.7}\text{Sr}_{0.3}\text{MnO}_3/\text{MgO}$, *only a continuous and small voltage drop is evidenced inside the grains down to the scale of 10–20 nm* (corresponding to our experimental resolution for the intra-grain voltage drops). The absence of additional intragrain resistance suggests that there is no static electronic phase separation in $\text{La}_{0.7}\text{Sr}_{0.3}\text{MnO}_3/\text{MgO}$ at 300 K. This aspect will be extensively discussed in a forthcoming communication.

In conclusion, we have demonstrated by local STP measurement that a large fraction of potential drops can occur at the grain boundaries, even in the case of epitaxial $\text{La}_{0.7}\text{Sr}_{0.3}\text{MnO}_3/\text{MgO}$ thin films with single-crystal-like transport properties. It has been directly shown by STP imaging that a significant part of the transport proceeds via a percolation between electrically well connected crystallites.

¹R. Mahesh, R. Mahendiran, A.K. Raychaudhuri, and C.N.R. Rao, *Appl. Phys. Lett.* **68**, 2291 (1996).

²H.Y. Hwang, S.-W. Cheong, N.P. Ong, and B. Batlogg, *Phys. Rev. Lett.* **77**, 2041 (1996).

³A. Gupta *et al.*, *Phys. Rev. B* **54**, R15 629 (1996).

⁴L.I. Balcells, J. Fontcuberta, B. Martinez, and X. Obradors, *Phys. Rev. B* **58**, R14 697 (1998).

⁵L. Ranno, A. Llobet, M.B. Hunt, and J. Pierre, *Appl. Surf. Sci.* **138**, 228 (1999); L. Ranno *et al.* (unpublished).

⁶N.D. Mathur *et al.*, *Nature (London)* **387**, 266 (1997).

⁷K. Steenbeck *et al.*, *Appl. Phys. Lett.* **71**, 968 (1997).

⁸S.P. Isaac, N.D. Mathur, J.E. Evetts, and M.G. Blamire, *Appl. Phys. Lett.* **72**, 2038 (1998).

⁹P. Murali and D. Pohl, *Appl. Phys. Lett.* **48**, 514 (1986).

¹⁰A.D. Kent, I. Maggio-Aprile, Ph. Niedermann, and Ø. Fischer, *Phys. Rev. B* **39**, 12 363 (1989); A.D. Kent *et al.*, *J. Vac. Sci. Technol. A* **8**, 459 (1989).

¹¹J.J. Versluijs, F. Ott, and J.M.D. Coey, *Appl. Phys. Lett.* **75**, 1152 (1999).

¹²M. Fäth *et al.*, *Science* **285**, 1540 (1999).